

Synthesis, characterization and biological applications of biofunctional gold nanoparticles for systemic circulation and biological sustainability

Manoj Kumar Goshisht*

Department of Chemistry, Dr. B. R. Ambedkar National Institute of Technology, Jalandhar, 144011, Punjab, India

*Corresponding author: Tel: (+91) 9582123259; E-mail: mkgh07@gmail.com

Received: 31 March 2016, Revised: 09 August 2016 and Accepted: 21 April 2017

DOI: 10.5185/amp.2017/690

www.vbripress.com/amp

Abstract

Designing nanomaterials for biomedical applications is not a trivial task. Avoidance of the immune system, stability in physiological media, and cell membranes, low toxicity, and optimal bioperformances are critical for the success of the designed nanomaterials. This review focuses on the study of protein-protein and protein-carbohydrates interactions. Most of the biological functions involving biochemical process are closely controlled by protein-protein interactions. Multi-protein complexes perform several catalytic functions. The review also focuses on the *in vitro* synthesis of bioconjugated nanoparticles and their biological applications such as antimicrobial agents and drug delivery vehicles. The synthesized nanoparticles act as sensor for such interactions. The *in vitro* synthesis of Au NPs also helps to understand such interactions with better clarity, which are otherwise elusive in the absence of NPs due to their highly complex nature. Both lysozyme (Lys) / Cytochrome, c (Cyt. c) and lysozyme/zein complexes showed remarkable surface adsorption on NP surfaces. The former system produced pH responsive NPs due to its amphiphilic nature and good antimicrobial properties while the latter system produced pH insensitive NPs due to its hydrophobic nature dominated by zein due to presence of non-polar amino acids such as leucine, alanine and proline. Due to insignificant hemolysis both systems may be used as drug delivery vehicles in systemic circulation. The diethylaminoethyl dextran chloride (DEAE) -protein interactions showed that DEAE-BSA and DEAE-Lys mixtures are amphiphilic whereas DEAE-zein mixture is hydrophobic in nature. All different complexes demonstrate strong surface adsorption on both presynthesized Au NPs as well as *in vitro* synthesis of Au NPs, which leads to the formation of biofunctional Au NPs best suited for biological applications in systemic circulation. The biological applicability is demonstrated from the hemolysis measurements where both DEAE-BSA as well as DEAE-Lys coated Au NPs do not show any marked hemolysis, thus proving to be the best suited vehicles for drug release in systemic circulation. DEAE-zein coated NPs, on the other hand, showed this behavior only in the DEAE rich region of the mixture, but in the protein rich region hemolysis dominates. Copyright © 2017 VBRI Press.

Keywords: Protein-protein interactions, bioconjugated nanoparticles, surface adsorption, hydrophilic and hydrophobic surface, hemolysis, antimicrobial agents and drug delivery vehicles.

Introduction

Recent developments in the field of colloidal science have extended our ability to fine tune the physicochemical properties of nanomaterials in order to achieve enhanced or novel magnetic, optical, and electronic properties when compared to their bulk counterparts. These features enable engineered nanomaterials to operate at the biomolecular level, with functions ranging from contrast for (multimodal) molecular imaging [1] to more complex tasks such as drug delivery, targeting, and therapy [2,3]. Bionanomaterials demonstrate tremendous potential due to their versatile applications in the biomedical field. Synthesis of such materials is usually a several steps cumbersome process that needs to tag bioactive molecules to nanomaterials for their appropriate use as biomarkers, drug release vehicles, or cytotoxic agents toward tumour

cells. Environmentally friendly green chemistry routes are required to explore their potential use in a wide range of applications. The physical and chemical properties of biomaterials can have a profound impact on cell proliferation and remodeling of tissues [4]. Bioactive molecules such as phospholipids [5-8] proteins [9-13], and other biopolymers [14], can be directly used in biomineralization to produce biofunctional materials. Biomineralization can also help us to understand how biomolecules control material properties such as nucleation, growth, shape, and composition. Little is known about their shape control effects because normally biomolecules are not directly used as shape-directing agents. Rather they have been used as linkers [15-17], sensors [18-20], or target-directing vehicles [21, 22]. Exploring their shape-directing ability especially of metal or semiconductor nanomaterials is another open field that

has been rarely exploited [6, 9, 12] probably due to their complex behavior which is usually not so simple to follow. In order to extract the full potential of biofunctional nanoparticles (NPs) in systemic circulation, understanding of their fundamental aspects at the molecular level is essential. Protein coated biofunctional NPs are promising vehicles for drug release in systemic circulation, but a fundamental understanding of protein adsorption and its ability to interact with the blood cells is an important aspect to be studied for their effective use.

Herein, we studied the potential of protein – protein and protein–dextran complex coated NPs as drug carriers in systemic circulation and present their fundamental properties essential to mark them suitable biological nanomaterials for their applications in pharmaceutical formulations. Protein–protein interaction [23–26] is the most important tool in understanding the fundamental basis of biophysical chemistry. Most of the biological functions involving biochemical processes are closely controlled by the protein–protein interactions. Usually multiprotein complexes perform several catalytic functions which are not in the preview of their components. Protein–protein interactions are involved in almost every biochemical process in a living cell. Information about these interactions is essential for the development of new therapeutic approaches toward different diseases as well as for their environmental applications.

We investigate the nature of complex formation by lysozyme with Cyt,c and zein to use these complexes to produce functionalized gold (Au) nanoparticles (NPs) for different biological applications. Lysozyme/Cyt,c complexation, apart from its expected antimicrobial activities, helped us to understand the mechanism of protein–protein interactions since both are well-known model proteins. Likewise, lysozyme combination with zein helped us to understand antimicrobial activities especially in food products such as biodegradable films and microcapsule formation where zein is frequently used. Zein is clear, odorless, tasteless, edible, and hence used in processed foods and pharmaceuticals. It contains high proportions of non-polar amino acid residues (such as leucine, alanine, and proline) which make it water insoluble [27, 28]. Lysozyme, a highly important model protein, is abundantly available in human tears, saliva, breast milk, and mucus, where it demonstrates its ability to kill bacteria by attacking peptidoglycans through the hydrolysis of glycosidic bonds [29–32]. Polymeric peptidoglycan consists of sugars and amino acids, which constitute the cell wall of bacteria. Cyt,c is another model protein, which is known for its electron exchange reactions and is highly capable of undergoing redox reactions [33]. BSA is composed of 580 amino acid residues with 17 interchain disulfide bonds. Protein–dextran complexes play a significant role in tissue morphogenesis, cell proliferation, signal transduction, infection, and therapeutics [34, 35]. Since such complexes are the result of weak intermolecular interactions, therefore, it is always difficult to detect them through complicated spectroscopic measurements.

Carbohydrates usually interact through weak amphiphilic or van der Waal's interactions with proteins. Such interactions can be magnified if an ionic polysaccharide such as diethylaminoethyl dextran chloride (DEAE) is used, which possesses greater ability to interact with water-soluble proteins [36, 37]. DEAE is one of the most versatile polysaccharides with promising applications [38, 39]. It has a high affinity for negatively charged DNA, while its cellulose counterpart is used in ion exchange chromatography, protein and nucleic acid purification, as well as separation [40, 41]. It is also used as an adjuvant in vaccine production [42, 43], enhancement of protein and nucleic acid uptake [44, 45], gene therapy [46], protein stabilizers [47], and flocculating agents [48, 49]. Its nontoxic nature allowed it to be used in oral formulations especially designed to decrease serum cholesterol and triglycerides. These applications are primarily related to its water-soluble nature based on amphiphilic behavior that arises from a neutral sugar backbone and charged quaternary amine side chains.

We studied the interactions of DEAE with different kinds of model proteins such as bovine serum albumen (BSA), lysozyme (Lys), zein, cytochrome c (Cyt, c) and carboxymethylcellulose (CMC) in the presence of AuNPs. Usually such interactions are very weak and complex, and it is not easy to detect and properly understand them. However, the presence of AuNPs magnifies them during the process of surface adsorption and allowed us to precisely understand them because protein and its complexes are highly prone to the surface adsorption, and the magnitude of the surface adsorption is further related to the DEAE–protein interactions. Such surface activity also leads to the formation of biofunctional NPs with interesting biological applications [50]. Lys and BSA are well-known model proteins, while zein is corn storage protein with several industrial applications. Lys coated NPs demonstrate wonderful antimicrobial activities [51], while BSA coated NPs are considered to be excellent vehicles for drug release in systemic circulation. Since zein is an edible protein, zein coated NPs can be easily used for various pharmaceutical formulations [52]. In combination with DEAE, DEAE–protein complex coated NPs are expected to provide even better applicability in order to understand the bioactive role of DEAE in various biological applications.

Our objective in this study is to understand the DEAE interactions with these proteins over the entire mixing range and to identify a suitable DEAE–protein mixture which best suits the synthesis of biofunctional Au NPs. Since each protein is a well understood model protein with specific applications, their complexes with DEAE would allow to produce biofunctional NPs with even better biological applications. Our next objective is to study folding and unfolding behavior, formation of nucleating centres and surface adsorption of proteins and protein-carbohydrate complexes.

In this review, we studied pathways for exploring such interactions by taking the advantage of synthesis of gold (Au) nanoparticles (NPs) *in vitro* in the presence of a

binary combination of proteins [53–58], where growing NPs act as sensors for such interactions. We studied that bioconjugated NPs thus produced depict the properties of the protein complexes and hence are best suited for drug delivery vehicles as well as antimicrobial agents.

Synthesis of biofunctional gold nanoparticles (AuNPs)

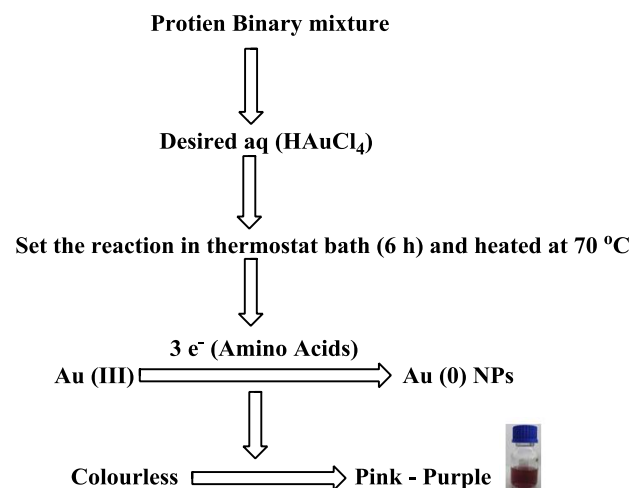


Fig. 1. Schematic representation of *in vitro* synthesis of Au NPs in protein – protein binary mixtures.

In vitro synthesis of biofunctional Au NPs in protein–protein binary mixtures

Binary mixtures of zein + BSA, zein + Cyt,c, Lys + Cyt, c and Lys + zein were made by taking each protein solution. Then, a desired amount of HAuCl₄ was added in 10 ml of each solution in screw-capped glass bottles and kept in a water thermostat bath (Julabo F 25) at precise 70 °C ± 0.1 °C for six hours under static conditions. The protein mixture especially in the unfolded state induced

by the high temperature [56–58] initiated the reduction of Au(III) into Au(0) due to its weak reducing ability and resulted in the color change from colorless to pink-purple. After six hours, the samples were cooled to room temperature and kept overnight. The NPs were purified from pure water at least three times to remove unreacted protein. These reactions were also simultaneously monitored under the effect of temperature variation by UV-visible and steady state fluorescence spectroscopy measurements in the wavelength range of 200–900 nm to observe the influence of the protein complex on the synthesis of Au NPs in terms of protein unfolding. Au NPs were characterized by Transmission Electron Microscopic (TEM) analysis on a JEOL 2010F at an operating voltage of 200 kV. The samples were prepared by mounting a drop of a solution on a carbon coated Cu grid and allowed to dry in the air.

In vitro synthesis of biofunctional Au NPs in DEAE–protein binary mixtures

Stock solutions of each component of binary mixtures of DEAE + BSA, DEAE + Lys, and DEAE + zein were made by dissolving in pure water (zein was aqueous solubilized by taking 24 mM SDS solution). This was followed by the mixing of the components to produce respective binary mixtures covering the entire weight fraction (W_{DEAE}) range by keeping the total amount constant. Then, HAuCl₄ was added in each weight fraction in screw-capped glass bottles and kept in a water thermostat bath (Julabo F25) at a precise 70 ± 0.1 °C for 6 h under static conditions. Each mixture initiated the reduction of Au(III) into Au(0) due to the weak reducing ability of both DEAE and protein that resulted in the color change from colorless to bright pink or pink-purple. After 6 h, the samples were cooled to room temperature and kept overnight. The NPs were purified from pure water at

Table 1. Chemicals used and their specifications.

Following chemicals were used

Chemicals	Brand	CAS Number	Purity
Bovine Serum Albumin (BSA) (Molar Mass 66 kDa)	Sigma-Aldrich, USA	9048-46-8	≥96.0%
Cytochrome,c (Cyt,c) from bovine heart muscle (molar mass 12 kDa)	Sigma-Aldrich, USA	9007-43-6	90%
Zein Protein (molar mass 21 kDa)	Sigma-Aldrich, USA	9010-66-6	-----
Lysozyme (molar mass) from chicken egg white (molar mass 14.3 kDa)	Sigma-Aldrich, USA	12650-88-3	≥90.0%
Diethylaminoethyl dextran chloride (DEAE) (molar mass 500.0 kDa)	Sigma-Aldrich, USA	9064-91-9	≥99.5%
Sodium dodecylsulfate (molar mass 288.38)	Sigma-Aldrich, USA	151-21-3	98.0%
Chloroauric acid (HAuCl ₄ .3H ₂ O) (molar mass 393.83)	Sigma-Aldrich, USA	16961-25-4	99.9%
Deoxyribonucleic acid (DNA) from horse (<i>Equuscaballus</i>) (molar mass 50.0 - 100.0 kDa)	Sigma-Aldrich, USA	9007-49-2	-----
Sodium borohydride (molar mass 37.83)	Sigma-Aldrich, USA	16940-62-2	≥98.0%
Ethidium bromide (molar mass 394.3) (An intercalating fluorescent dye reagent for DNA/RNA staining)	Sigma-Aldrich, USA	1239-45-8	~95%
Sodium citrate. 2H ₂ O (molar mass 294.10)	Santa Cruz Biotech, USA	6134-04-3	≥99.0%

Double distilled water was used for all sample preparations.

least three times to remove unreacted protein. In the second method, calculated amounts of presynthesized citrate stabilized Au NPs were taken in small UV-visible cuvettes. The size of the Au NPs was 11 ± 3 nm with a zeta potential of -18.5 ± 1.7 mV. The constant amount of Au NPs was titrated with a freshly prepared DEAE-protein mixture at 20 and 70 °C. At 20 °C, the protein was considered to be in the folded state when it interacted with DEAE, while at 70 °C it acquired maximum unfolding. The DEAE-protein complex demonstrated dramatic surface adsorption on NPs and was simultaneously monitored by the spectroscopic analysis.

Synthesis of bifunctional Au NPs by using presynthesized Au NPs

In this method, calculated amounts of presynthesized citrate stabilized Au NPs were taken in small UV-visible cuvettes. The size of the Au NPs was 11 ± 3 nm with a zeta potential of -18.5 ± 1.7 mV. They were titrated with a freshly prepared DEAE-protein mixture by keeping constant the amount of Au NPs at 20 and 70 °C. At 20 °C, the protein was considered to be in the folded state when it interacted with DEAE, while at 70 °C it acquired maximum unfolding. The DEAE-protein complex demonstrated dramatic surface adsorption on NPs and was simultaneously monitored by the spectroscopic analysis.



Fig. 2. Synthesis of Au NPs and adsorption of DEAE-protein mixture on citrate stabilized Au NPs.

Methods used to characterize the bifunctional AuNPs

Spectroscopic analysis

UV-visible (Shimadzu, model no. 2450, double beam) and steady state fluorescence spectroscopy (PTI Quanta Master) measurements in the wavelength range of 200–900 nm were employed to simultaneously monitor the reactions under the effect of temperature and reaction time to observe the influence of protein complex on the synthesis of Au NPs in terms of protein unfolding and subsequent protein-protein interactions. Both instruments were equipped with a TCC 240A thermoelectrically temperature controlled cell holder that allowed measurement of the spectrum at a constant temperature within ± 1 °C.

Microscopy

Protein coated Au NPs were characterized by transmission electron microscopic (TEM) analysis on a JEOL 2010F at an operating voltage of 200 kV. The samples were prepared by mounting a drop of a solution

on a carbon coated Cu grid and allowed to dry in the air. The morphology and particle size of protein coated AuNPs were further determined by scanning electron microscopy (SEM) and atomic force microscopy (AFM).

Dynamic light scattering (DLS)

DLS measurements were applied for determination of particles size distribution. DLS measurements were performed using a light scattering apparatus (Zetasizer, Nano series, Nano-ZS, Malvern Instruments) equipped with a built-in temperature controller with an accuracy of ± 0.1 °C. The measurements were made using a quartz cuvette with a path length of 1 cm. Averages of 10 measurements were analyzed using the standard algorithms with an uncertainty of less than 7%.

X-ray diffraction (XRD)

XRD was employed for the determination of crystallinity. The X-ray diffraction (XRD) patterns were characterized with graphite monochromatized Cu $K\alpha$ irradiation.

Molecular dynamics (MD) simulations

The MD simulations were performed in periodic boundary conditions using the GROMACS (Groningen Machine for Chemical Simulations) program (version 4.6.5) [59], and the OPLS-AA (Optimized Potentials for Liquid Simulations) force field was used to describe the system. For protein-gold interactions, the recently developed GoIP force field [60] was parametrized on the basis of density functional calculations and experimental data including a term describing metal polarizability [61]. The 4.5 ns conventional molecular dynamics simulation of Cyt,c and lysozyme in the temperature range from 310 to 350 K was employed to analyze the interactions between the two proteins, and their structures were obtained from the protein data bank at Brookhaven [62] with entry codes 3NWV and 2LYZ, respectively. Before MD simulations, the models of proteins were solvated with the explicit SPC (simple point charge) water [63] embedded in $1.4 \text{ nm} \times 1.4 \text{ nm} \times 1.4 \text{ nm}$ box. The system was subjected to a steepest descent energy minimization until a tolerance of 1000 kJ/mol step by step. First, an NVT (constant number of atoms, volume, and temperature) simulation was performed to bring the system to the target temperature, followed by an NPT (constant number of atoms, pressure, and temperature) simulation to allow the system to find the correct density. Temperature coupling was performed using the Nose-Hoover thermostat, which produced a more correct ensemble of kinetic energies than the Berendsen method. All bond lengths including hydrogen atoms were constrained by the LINCS (Linear Constraint Solver) algorithm [64]. The electrostatic interactions were calculated by using the Particle-Mesh Ewald (PME) algorithm [65]. The cutoff for van der Waals interactions was 0.9 nm.

Hemolytic assay

Hemolytic assay was performed to evaluate the response of protein-conjugated NPs on blood group B of red blood cells (RBCs) from a healthy human donor. Briefly, a 5% suspension of RBCs was used for this purpose after three washings along with three concentrations (i.e. 25, 50, and $100 \mu\text{g ml}^{-1}$) of each NP sample. The positive control was RBCs in water and it was prepared by spinning 4 ml of 5% RBCs suspension in PBS. PBS as the supernatant was discarded and the pellet was resuspended in 4 ml of water. The negative control was PBS. All the readings were taken at 540 nm i.e. absorption maxima of hemoglobin.

Microbiological evaluation

Antifungal activities of bioconjugated NPs were evaluated using disc-diffusion test for pre-screening of the antifungal potential of agents and the broth micro-dilution method to determine the minimum inhibitory concentration (MIC). The following fungal strains were used: *Aspergillus niger* (MTCC-281), *Candida geotrichum* (MTCC-3993), *Candida albicans* (MTCC-227) and *Candida tropicalis* (MTCC-230). Fungi were cultivated at 25°C on Sabouraud Dextrose Agar (SDA) and MIC was determined by using Sabouraud Dextrose Broth (SDB). The samples and standard were suspended in dimethylsulfoxide (DMSO) and applied in different concentrations. DMSO was used as a negative control and an antifungal drug (fluconazole) as positive control.

Antifungal activity

The disk-diffusion assay was applied to determine the growth inhibition of fungi by protein conjugated NPs. Overnight fungal cultures were spread onto SDA. The NP samples were applied to 8 mm disks (Whatman paper No. 1). After 48 h of incubation at 25°C , the diameter of growth inhibition zones was measured.

MIC determination

The broth dilution test was performed in test tubes. The conidial suspension, which gave the final concentration of 1×10^5 CFU per ml, was prepared. A growth control tube and sterility control tube were used in each test. After 24–72 h incubation at 25°C , the MIC was determined visually as the lowest concentration that inhibits growth, evidenced by the absence of turbidity.

DEAE-protein interactions using pre-synthesized Au NPs

The interactions were determined by titrating fixed weight fractions (W_{DEAE}) of DEAE-protein mixtures with 1 mM citrate stabilized Au NPs (average size = 11 ± 3 nm and zeta potential = -18.5 ± 1.7 mV). Fig. 3a demonstrates a typical UV-visible scan of such a titration of the DEAE-BSA mixture with $W_{\text{DEAE}} = 0.4$ at 20°C . Presynthesized Au NPs gave a sharp absorbance close to 515 nm [66] due to the surface plasmon resonance (SPR).

A systematic addition of $W_{\text{DEAE}} = 0.4$ initially led to an increase in this absorbance with a regular blue shift due to the greater colloidal stabilization achieved by the Au NPs upon the adsorption of a DEAE-BSA complex on the NP surface [67]. After a certain concentration, the intensity of the absorbance started decreasing with no more blue shift. Fig. 3b explained the variation of both intensity as well as wavelength with respect to the total concentration of the DEAE-BSA complex at 20°C .

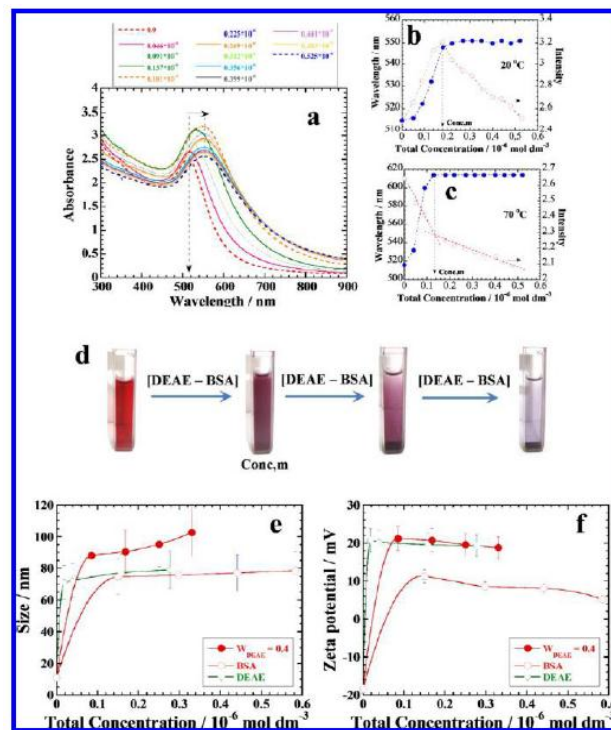


Fig. 3. (a) Plots of UV-visible absorbance of presynthesized Au NPs upon the systematic addition of a DEAE-BSA mixture with $w_{\text{DEAE}} = 0.4$ at 20°C . Notice the red shift as well as decrease in the intensity with the increase in the [Total DEAE-BSA]. (b and c) Variation in the intensity and wavelength of the absorbance of Au NPs at 20 and 70°C , respectively. (d) Series of photographs of color change of Au NPs suspension in UV-visible cuvette upon increasing the amount of DEAE-BSA. The color change from the first cuvette to the last one occurs over a period of few hours. (e) Plots of size/nm and (f) zeta potential of DEAE-BSA coated Au NPs with concentration from DLS measurements for $w_{\text{DEAE}} = 0.4$, DEAE, and BSA at 20°C .

Intensity passed through a strong maximum where wavelength reaches a constant value. The maximum indicated the “minimum concentration of the complex” (Conc,m) required to fully stabilize the 1 mM Au NPs. Beyond Conc,m, self-aggregation among the coated NPs diminished the intensity. The same reaction at 70°C induced an instant reduction in the intensity with a blue shift (Fig. 3c) due to the self-aggregation of Au NPs in view of the instant surface adsorption of the DEAE-BSA complex because BSA was in its unfolded state at 70°C [68], and hence the complex was highly surface active. A break in the intensity profile with a larger slope coincided with the wavelength profile where no more blue shift was observed. This break point provided the “Conc,m” value at 70°C . This caused a dramatic color change of Au NPs

from bright red to purple in each sample at both 20 and 70 °C, which eventually led to a complete coagulation of Au NPs as depicted in **Fig. 3d**. DLS measurements indicated a dramatic size increase of Au NPs upon the DEAE–protein complex adsorption (**Fig. 3e**). BSA and DEAE alone as well as their mixtures instantaneously led to a size increase of Au NPs initially, which was relatively very prominent for the DEAE–BSA mixture rather than for BSA or DEAE alone. This demonstrated that the complex was clearly more surface active than either of the components. Likewise, zeta potential measurements indicated that an initial DEAE–protein complex adsorption was driven by strong electrostatic interactions. Citrate stabilized Au NPs were negatively charged with a zeta potential of -18.5 ± 1.7 mV. The addition of the DEAE–BSA complex converted the negative zeta potential value into a large positive value which subsequently showed a small decrease with the increase in the amount of DEAE–BSA due to subsequent deposition of more layers which might cause the screening of charged sites. There was also little difference between the zeta potential values for the DEAE and DEAE–BSA mixture, suggesting the fact that the positive charge of the complex was mainly contributed by the cationic DEAE.

Molecular dynamics (MD) simulations of DEAE – Protein Interactions

In this section, we studied the results of atomistic simulations on the interactions of DEAE with BSA, Lys, and zein, as well as their complexes with the Au NP surface. The stability of DEAE–BSA and DEAE–Lys complexes was tested by simulating it for 5 ns at 310 K. Visual inspection of the trajectory confirmed that DEAE made favorable interactions with BSA, while the contact with Lys did not last up to the end in all the simulations. The total energy of the simulation model of the DEAE–BSA complex versus simulation time at 310 K gave an indication of the overall stability of the MD trajectory. The interaction energy between DEAE and BSA was described by two main terms, i.e., van der Waals energy and electrostatic energy. The results showed that the electrostatic interactions played a more important role than the van der Waals interactions, which allowed DEAE to interact strongly with predominantly negatively charged BSA. Furthermore, the number of hydrogen bonds formed increased between DEAE and BSA, whereas it remained almost the same with Lys. These interactions were explained well from the electrostatic potential map by using an adaptive Poisson–Boltzmann [69] approach on the solvent accessible surface of this system.

Protein–Gold Surface (NP) Interactions

Interactions between the protein and solid surface are at the heart of many potential applications in bio nanotechnology [70] and medicine, [71] where we need to understand which amino acid, peptide, or protein binds favorably to a given solid surface. MD studies helped to

locate specific amino acid residues which drive such interactions. The peptide chains were selected i.e., peptide 1 for BSA (GLU-LYS-LYS-PHE-TRP-GLY-LYS-TYR-LEUTYR- GLU-ILE-ALA-ARG-ARG-HIS) and peptide 2 for Lys (VAL-SER-ASP-GLY-ASN-GLY-MET-ASN-ALA-TRP-VALALA- TRP-ARG-ASN-ARG-CYS-LYS) to understand their interactions with the Au surface in the presence of DEAE.

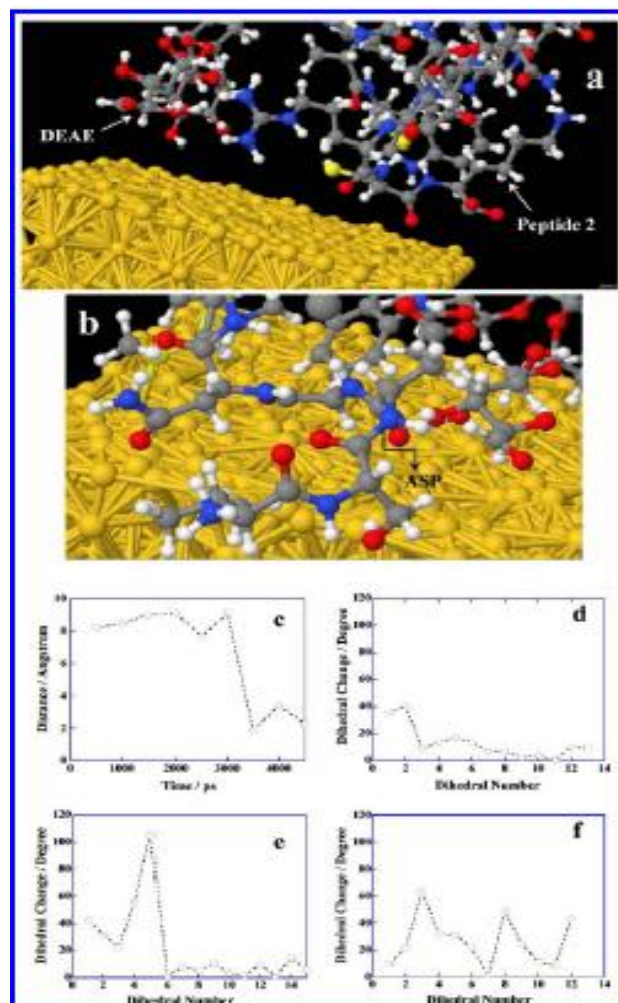


Fig. 4. (a) Snapshot of a DEAE and peptide 2 complex on the surface of gold slab. (red, O; blue, N; white, H; yellow, S; black, C). (b) Specific location of ASP. In both figures, water molecules and ions have been omitted for the sake of clarity. (c) Distance of amino acid residue ASP with time from the gold slab. (d) Changes in α -carbon dihedral angles of peptide 1, (e) peptide 2, and (f) zein chain. The change is calculated as the difference between the average dihedral in the first and last 500 ps. Dihedral n corresponds to dihedral angle formed by α carbons n , $n + 1$, $n + 2$, and $n + 3$. Reproduced with permission from ACS.

These chains along with DEAE were placed on the top of the gold slab mimicking the surface of a NP. Peptide 2 interacted with the Au surface through MET, TRP, CYS, GLY, SER, ARG, and ASP, while peptide 1 interacted via LYS, HIS, TRP, ARG, and TYR [71,72]. Generally, CYS showed strong binding with the Au surface while other residues obeyed the following order: His \approx Trp > Met > (Tyr, Lys, Arg). ASP, which contributed to the maximum

negative potential for BSA, not showed the strong potential to bind the Au surface [72,73]. However, in the presence of DEAE, ASP played a governing role to help both BSA as well as Lys interact with the Au surface because ASP underwent electrostatic interactions with cationic DEAE. **Fig. 4a** and **b** showed this specifically for Lys where ASP helped in anchoring peptide 2 to the gold surface, and its approach to the gold surface was plotted in **Fig. 4c**. It was further explained on the basis of a change in the dihedral angles of peptide 1 (**Fig. 4d**) and peptide 2 (**Fig. 4e**). A change in the dihedral angles indicated a conformational change in the peptide upon its binding to the Au surface. The maximum change in dihedral angle occurred in the region where ASP was located in peptide 2 (**Fig. 4e**), whereas **Fig. 4d** which lacks ASP for peptide 1 (especially chosen to show the effect of ASP) not showed this drastic change.

Interactions between lysozyme/ cyt,c and lysozyme/zein through in vitro synthesis of Au NPs

In this section we studied the interactions between lysozyme / Cyt,c and lysozyme / zein using the *in vitro* synthesis of Au NPs as an indicator under the effect of temperature variation. Without Au NPs, these interactions were not visible, and there was no change in the absorption spectra of both mixtures. However, in vitro synthesis of Au NPs in the mixtures showed marked changes.

Isoelectric Point (pI)

The pI of adsorbed protein on the NP surface helped in understanding the nature of the lysozyme/Cyt,c complex. The pH of the as prepared sample was found close to 2.5, due to the dissociation of HAuCl₄ in the aqueous phase. Thus, low pH provided positive charge to the protein because the pI of lysozyme and Cyt,c was close to 11[74,75] and 10 [76], respectively. Adsorption of predominantly positively charged protein on the NP surface neutralized the positive charge and left the protein coated NPs with negative charge. This was confirmed from the gel electrophoresis where the protein coated NPs moved through the agarose matrix toward the positively charged electrode (**Fig. 5a**). When the protein stabilized colloidal suspension of Au NPs (ruby red color) was subjected to change in the pH, the absorbance at 540 nm decreased with the rise in pH due to the self-aggregation of protein coated NPs close to pH \approx 10 (**Fig. 5b**). It eliminated the ruby red color (see the color of the colloidal suspension in respective bottle), which reappeared to some extent after pH \approx 10. Thus, pH \approx 10 was found the pI of the lysozyme/Cyt,c complex that coated the NP surface. As the protein coating acquired the neutral charge close to pH \approx 10, it eliminated the electric double layer responsible for the colloidal stability with the result that nonpolar interactions predominated which led to the self-aggregation. The presence of the protein coating was clearly visible from the TEM images (**Fig. 5c, d**) where mostly hexagonal Au NPs of 37 ± 9 nm

were coated with ~ 5 nm thick protein coating (**Fig. 5d**). Thus, the results clearly indicated formation of lysozyme/Cyt,c complex and its adsorption on Au NPs.

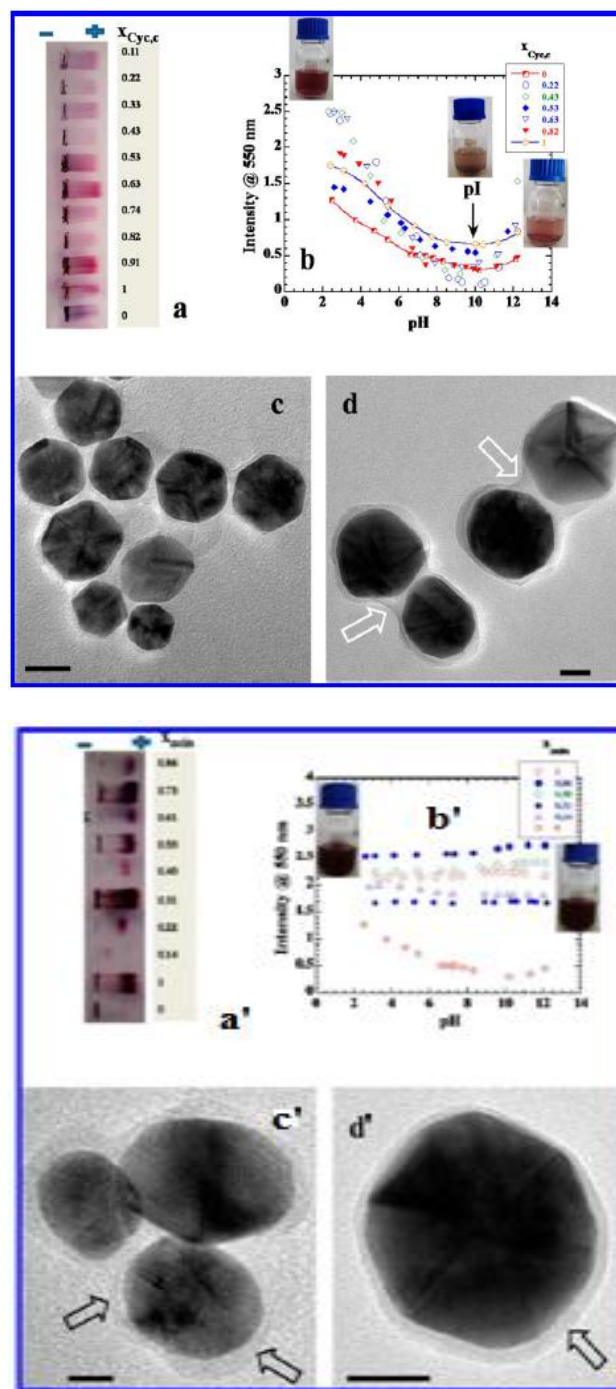


Fig. 5. (a and a') Gel electrophoresis of protein coated Au NPs synthesized with various mole fractions of lysozyme/Cyt,c and lys/zein mixtures, respectively. (b, and b') Variation of the intensity of protein coated Au NPs made with different mole fractions of lysozyme/Cyt,c and Lys/zein mixtures respectively, with pH. Photographs of reaction bottles show the change in the color of the NP colloidal suspension with pH. (c and d) TEM micrographs of protein coated Au NPs in large groups and pairs with scale bar of 20 nm, respectively. Block arrows indicate the protein coating in the form of thin film. Hydrophilic and hydrophobic surface of the space filled Cyt,c and lysozyme protein complex. Reproduced from ref. no. [50] with permission from ACS.

Gel electrophoresis further supported the predominance of zein in the lysozyme/zein complex. Because of the acidic reaction conditions, protein coated NPs acquired negative charge since the pI's of lysozyme and zein were around 11[74,75] and 7, [77] respectively, and hence the NPs moved toward the positive terminal of the battery (Fig. 5a). However, these NPs were nonresponsive to the pH change (except that of pure lysozyme) with no change in the ruby red color (Fig. 5b, see the color of the colloidal suspension at respective pH scale ends) and not showed any change in the absorbance with pH in contrast to Fig. 5b although the protein coating was clearly visible in TEM images (Fig. 5c' and d') just like that of Fig. 5c, d. The non-pH-responsive behavior of lysozyme/zein coated NPs primarily originated from the highly hydrophobic nature of zein as well as the overall negative charge provided by the SDS molecules, because zein was solubilized in 24mM SDS solution. This much SDS was sufficient for the solubilization of zein but not for its complete unfolding as reported by Deo et al [43]. Therefore, no uncomplexed SDS was expected in the aqueous solution, the presence of which could affect the unfolding behavior of lysozyme. Thus, SDS was the most appropriate choice in comparison to other mild conventional surfactants (because of its already reported data[78] on solubilization of zein) to study the protein-protein interactions in aqueous phase. Fig. c indicated the hydrophilic and hydrophobic surfaces of lysozyme/ Cyt,c

mixture where green color showed hydrophilic whereas orange color indicated hydrophobic surface.

Control of shape of Au NPs by protein mixture

The microscopic studies of lysozyme/ Cyt,c system showed thick layer of protein mixture on the NPs surface for various mole fractions indicated by block arrow (Fig. 6. b, c). The results showed an active involvement of protein mixtures in the NP stabilization as well as its shape control effects which produced mostly roughly spherical morphologies of 20–30 nm. Thus, nucleation was facilitated as well as closely controlled by the adsorption of unfolded protein on the NP surface which further promoted the protein seeding and hence accelerated protein-protein interactions. [79–81].

TEM images of Au NPs produced in the presence of binary mixtures of zein + Cyt,c (Fig. 6, d-f) showed contrasting differences from that of zein + BSA (Fig. 6, a-c). The mixture of zein + BSA (Fig. 6, a-c) produced mostly roughly spherical shapes of Au NPs much smaller size with substantial surface coating while mixture of zein + Cyt,c (Fig. 6, d-f) produced mostly flat triangles of 83 ± 17 nm size along with much smaller faceted Au NPs of different shapes, and no protein coating was seen. Further, in the presence of Cyt,c rich region (Fig. 6, e, f) production of larger aggregates of dendritic growth with practically no shape control effects were observed.

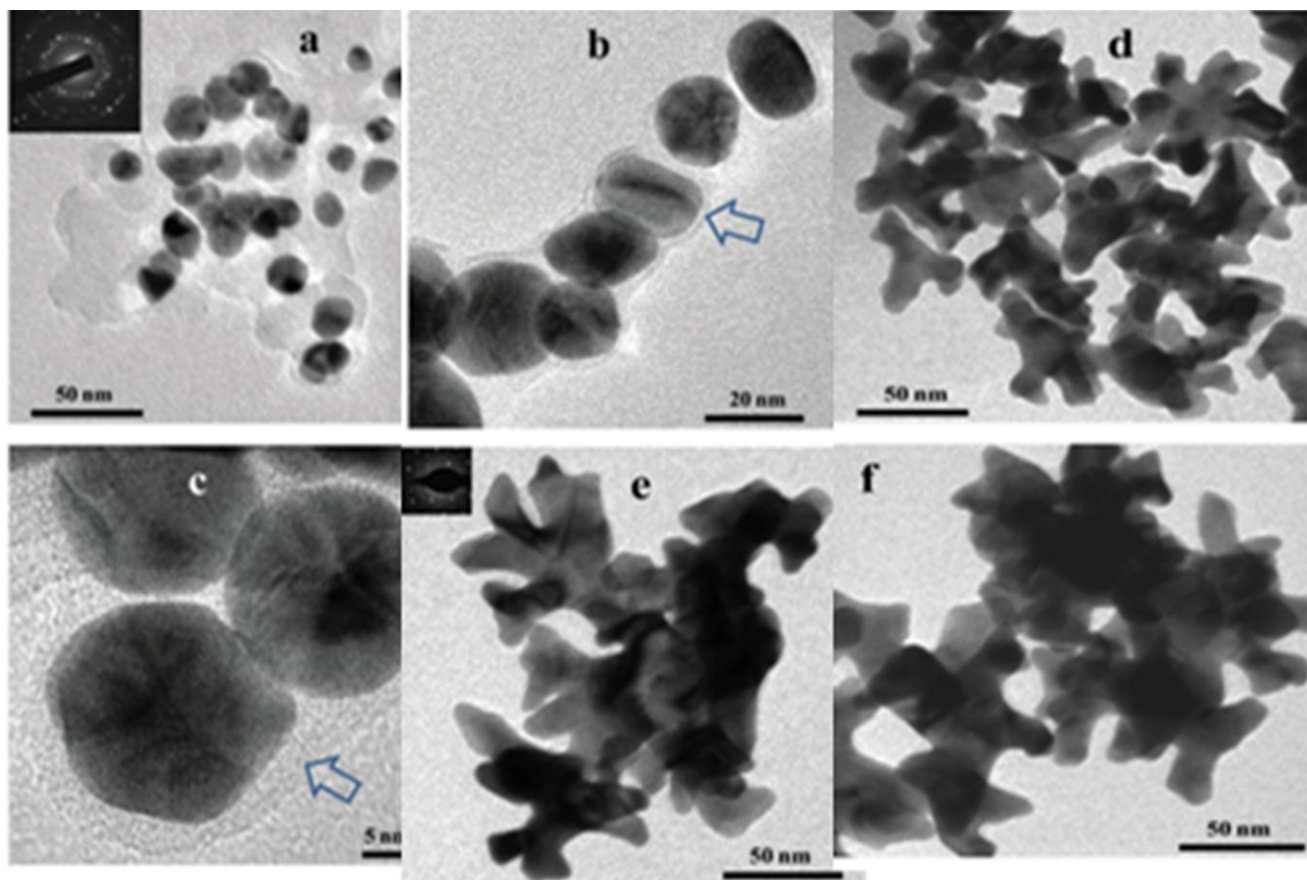


Fig. 6. (a-c) TEM images of Zein + BSA, whereas (d-f) TEM images of Zein + Cyt,c.

Hemolysis of zein + BSA and zein + cyt,c systems

Results of hemolysis of Au NPs prepared over the entire mole fraction range of both mixtures were tested and presented in percentage hemolysis = (sample absorbance \times negative control absorbance) / (positive control absorbance \times negative control absorbance) \times 100. **Fig. 7a** showed typical absorbance profiles of different doses of a purified sample along with the positive and negative controls. **Fig. 7b** illustrated the variation in the hemolysis of all samples of both mixtures. A clear difference between the sets of data for zein + BSA and zein + Cyc,c is evident. Three doses of zein + BSA conjugated NPs (i.e. 25, 50, and 100 $\mu\text{g ml}^{-1}$) showed almost insignificant hemolysis with little difference, whereas zein + Cyc,c coated AuNPs showed pronounced hemolysis in the Cyc,c rich region of the mixture which further showed dependence on the dose of NPs. Significant hemolysis was the consequence of several factors [82,83], which included highly anisotropic dendritic growth with large surface area and practically little protein coating which made hemolysis a thermodynamic favorable process to interact with the cell membrane through predominantly naked metal surface (**Fig. 7c**). The results showed that a greater dose of NPs of 100 $\mu\text{g ml}^{-1}$ with least protein coating showed maximum hemolysis in comparison to smaller doses. This proved the close correlation between the NP stabilization by the protein surface adsorption and hemolysis. Thus, zein + BSA coated NPs were considered to be the better model for their role as drug release vehicles in comparison to zein + Cyc,c coated NPs.

Antimicrobial studies of zein + BSA and zein + cyt,c systems

The wide applicability of zein in food and pharmaceutical industry prompted us to study the antimicrobial activities of the present protein coated NPs in order to improve the shelf life of the pharmaceutical formulations of such NPs. Four kinds of strains (see in methods) were selected for this study. We studied the Au NP samples prepared over the entire mole fraction of zein + BSA and zein + Cyc,c mixtures for their antimicrobial activities against these four strains and the results were presented in **Fig. 8a** and **Fig. 8b**, respectively. A dotted red line in both figures represented the minimum inhibitory concentration (MIC) [84,85] of an antifungal drug (fluconazole) as control. Fluconazole is a drug used in the treatment and prevention of superficial and systemic fungal infections. In comparison to this drug though all the samples of protein conjugated NPs needed much higher MIC, the concentration range in micrograms allowed to put them in the category of moderately antifungal agents. This was certainly an advantage in addition to their role in the pharmaceutical formulations where antimicrobial activities helped to improve their functionalities against the common yeast infections as well as their shelf life.

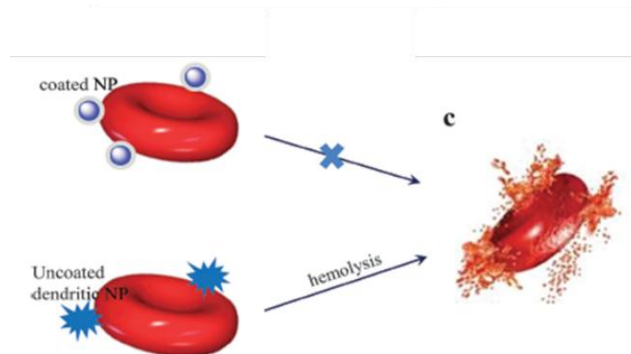
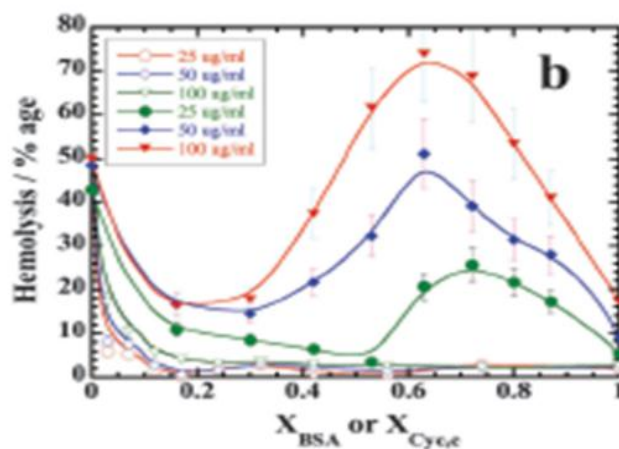
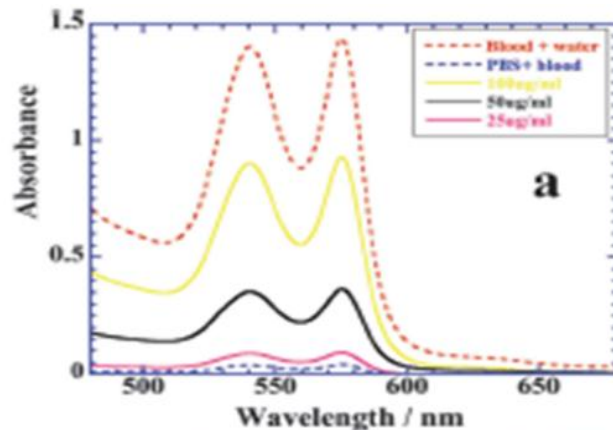


Fig. 7. (a) Absorbance profiles of hemolysis exhibited by different doses of Au NPs prepared with a reaction of mole fraction of Cyt,c. Photos show the extent of hemolysis for these samples with +ive and -ive controls. (b) Variation in the percentage hemolysis by Au NPs with different doses prepared over the entire mole fraction of zein + BSA (empty symbols) and zein + Cyc,c (filled symbols) mixtures. (c) Schematic depiction of the effect of shape, size, and protein coating on the hemolysis. Roughly spherical small NPs coated with protein not induced hemolysis in comparison to large dendritic NPs without protein coating. Reproduced from Ref. [51] with permission from the PCCP Owner Societies.

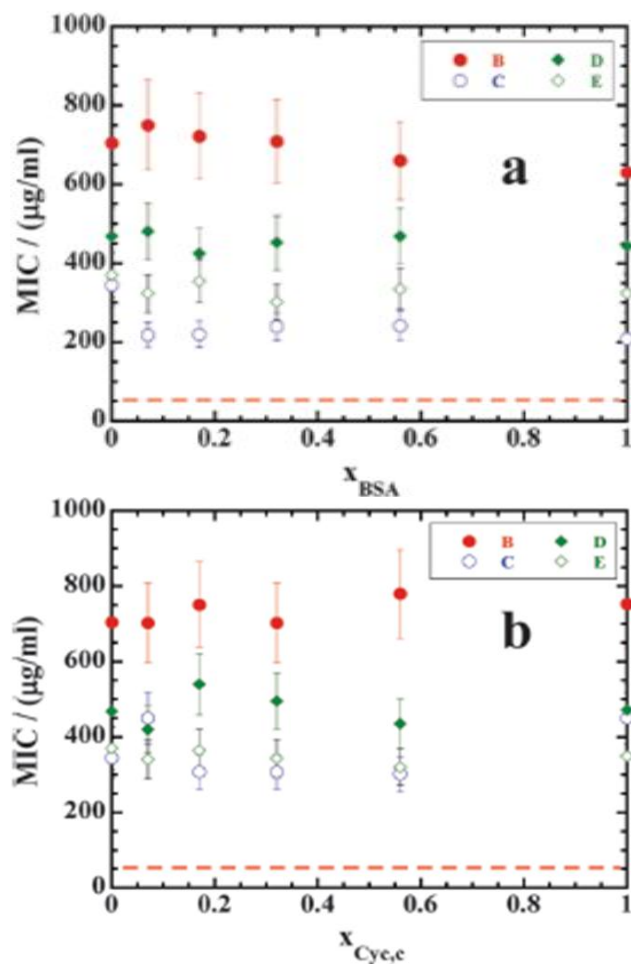


Fig. 8. Plots of minimum inhibitory concentration (MIC) of protein coated Au NPs of zein + BSA (a) and zein + Cyc,c (b) mixtures over the whole mole fraction range for *Aspergillusniger* (B), *Candidumgeotrichum* (C), *Candida albicans* (D) and *Candida tropicalis* (E). Dotted lines in both figures represents the MIC for the antifungal drug ‘Fluconazole’ as control. Reproduced from Ref. [51] with permission from the PCCP Owner Societies.

Conclusion and future perspectives

Variation The present results focused on the protein–protein interactions between the components of highly important model proteins and the simultaneous synthesis of protein coated Au NPs with wide industrial applicability. The studies showed remarkable DEAE–protein interactions which were predominantly amphiphilic in the case of DEAE–BSA and DEAE–Lys mixtures, whereas they were nonpolar in the case of DEAE–zein mixtures. All different complexes demonstrated strong surface adsorption on both presynthesized Au NPs as well as *in vitro* synthesis of Au NPs, which led to the formation of biofunctional Au NPs best suited for biological applications in systemic circulation. The biological applicability was demonstrated from the hemolysis measurements where both DEAE–BSA as well as DEAE–Lys coated Au NPs not showed any marked hemolysis, thus proved to be the best suited vehicles for drug release in systemic circulation.

DEAE–zein coated NPs, on the other hand, showed this behavior only in the DEAE rich region of the mixture. Electrostatic interactions between DEAE–BSA/Lys induced the unfolding in the protein with the result that several Au selective amino acid residues got a chance to interact with the Au surface and, hence, facilitated the surface adsorption of the DEAE–protein complex on Au NPs. Interactions between DEAE and zein were mainly triggered by the nonpolar amino acid residues like SER and GLN through hydrogen bonding, which consequently produced a predominantly nonpolar DEAE–zein complex. Both lysozyme + Cyt,c and lysozyme + zein complexes showed remarkable surface adsorption on NP surfaces that produced pH responsive NPs for the former system due to its amphiphilic nature and pH insensitive NPs for the latter due to its predominantly hydrophobic nature. The study concluded that zein demonstrated strong interactions with BSA throughout the mole fraction range whereas such interactions were limited to the zein rich region with Cyc,c. BSA interacted with zein through both electrostatic as well as hydrophobic interactions whereas Cyc,c predominantly demonstrated electrostatic interactions. Both zein + BSA as well as zein + Cyc,c complexes simultaneously adsorbed on the growing AuNPs and hence they controlled their shape and hence mostly spherical NPs were produced in the former case while poor coating of the latter generated large dendritic NPs. The Au NPs coated with zein + BSA complexes proved to be fine vehicles for drug release in systemic circulation because of their negligible hemolysis almost throughout the whole mole fraction range. This was not the case with the zein + Cyc,c complex coated NPs, which showed significant hemolysis in the Cyc,c rich region. Interestingly, NPs coated with the complexes of both mixtures showed an almost same degree of antimicrobial activities against four prominent strains which were frequently available in the food products and caused yeast infections. Hence, the formulations made of such protein coated NPs showed dual advantages as drug release vehicles and antimicrobial activities which was usually a rare combination for a formulation for biological applications. Bio-nanomaterials synthesis is one of the most fascinating branches of nanotechnology which is related to a mutual synergism between materials science and biology.

Nan-bio-devices and chips will pave the way for best and durable solutions of many critical illnesses related to cardiovascular diseases and cancer problems. Thus, nanoscale size drug delivery systems may revolutionize the entire drug therapy strategy and bring it to a new height in near future. However, toxicity concerns of the nanosize formulations should not be ignored. Full proof methods should be established to evaluate both the short-term and long-term toxicity analysis of the nanosize drug delivery systems.

Notes

The author declares no competing financial interest.

Acknowledgements

M. K. G. thankfully acknowledges the financial support provided by the CSIR [ref no: 01(2683)/12, ref no: 01(2700)/12/EMR-II].

References

1. Erathodiyil, N.; Ying, J. Y. *Acc. Chem. Res.* **2011**, 44, 925–935.
2. Faraji, A. H.; Wipf, P. *Bioorg. Med. Chem.* **2009**, 17, 2950–2962.
3. Kievit, F. M.; Zhang, M. *Acc. Chem. Res.* **2011**, 44, 853–862.
4. Langer, R.; Tirrel, D. A. *Nature*. **2004**, 428, 487–92.
5. Bakshi, M. S.; Possmayer, F.; Petersen, N. O. *Chem. Mater.* **2007**, 19, 1257.
6. Bakshi, M. S.; Possmayer, F.; Petersen, N. O. *J. Phys. Chem. C*. **2007**, 111, 14113.
7. Bakshi, M. S.; Kaur, G.; Thakur, P.; Banipal, T. S.; Possmayer, F.; Petersen, N. O. *J. Phys. Chem. C*. **2007**, 111, 5932–40.
8. Meister, A.; Drescher, S.; Mey, I.; Wahab, M.; Graf, G.; Garamus, V. M.; Hause, G.; Mogel, H. J.; Janshoff, A.; Dobner, B.; Blume, A. *J. Phys. Chem. B*. **2008**, 112, 4506.
9. Bakshi, M. S.; Thakur, P.; Kaur, G.; Kaur, H.; Banipal, T. S.; Possmayer, F.; Petersen, N. O. *Adv. Funct. Mater.* **2009**, 19, 1451.
10. Bakshi, M. S.; Jaswal, V. S.; Kaur, G.; Simpson, T. W.; Banipal, P. K.; Banipal, T. S.; Possmayer, F.; Petersen, N. O. *J. Phys. Chem. C*. **2009**, 113, 9121.
11. Bakshi, M. S.; Kaur, H.; Banipal, T. S.; Singh, N.; Kaur, G. *Langmuir*. **2010**, 26, 13535.
12. Bakshi, M. S.; Kaur, H.; Khullar, P.; Banipal, T. S.; Kaur, G.; Singh, N. *J. Phys. Chem. C*. **2011**, 115, 2982.
13. Xie, J.; Lee, J. Y.; Wang, D. I. C. *J. Phys. Chem. C*. **2007**, 111, 10226.
14. Wu, L.; Shi, C.; Tian, L.; Zhu, J. *J. Phys. Chem. C*. **2008**, 112, 319.
15. Dave, N.; Liu, J. *ACS Nano*. **2011**, 5, 1304.
16. Faure, A. C.; Hoffmann, C.; Bazzi, R.; Goubard, F.; Pauthe, E.; Marquette, C. A.; Blum, L. J.; Perriat, P.; Roux, S.; Tillement, O. *ACS Nano*. **2008**, 2, 2273.
17. Aili, D.; Enander, K.; Baltzer, L.; Liedberg, B. *Nano Lett.* **2008**, 8, 2473.
18. Willner, I.; Willner, B. *Nano Lett.* **2010**, 10, 3805.
19. Hall, W. P.; Ngatia, S. N.; Van Duyn, R. P. *J. Phys. Chem. C*. **2011**, 115, 1410.
20. Lowe, L. B.; Brewer, S. H.; Krämer, S.; Fuierer, R. R.; Qian, G.; Agbasi-Porter, C. O.; Moses, S.; Franzen, S.; Feldheim, D. L. *J. Am. Chem. Soc.* **2003**, 125, 14258.
21. Kaittanis, C.; Santra, S.; Perez, J. M. *J. Am. Chem. Soc.* **2009**, 131, 12780.
22. Dreaden, E. C.; Mwakwari, S. C.; Sodji, Q. H.; Oyelere, A. K.; El Sayed, M. A. *Bioconjugate Chem.* **2009**, 20, 2247.
23. Oncley, J. L.; Ellenbogen, E.; Gitlin, D.; and Gurd, F. R. N. *J. Phys. Chem.* **1952**, 56, 85–92.
24. Rakickas, T.; Gavutis, M.; Reichel, A.; Piehler, J.; Liedberg, B.; and Valiokas, R. A. *Nano Lett.* **2008**, 8, 3369–3375.
25. Elcock, A. H.; Sept, D.; and McCammon, J. A. *J. Phys. Chem. B*. **2001**, 105, 1504–1518.
26. del Pino, P.; Pelaz, B.; Zhang, Q.; Maffre, P.; Nienhaus, G. U.; and Parak, W. J. *Mater. Horiz.* **2014**, 1, 301–313.
27. Wu, S. W.; Myers, D. J.; and Johnson, L. A. *Cereal Chem.* **1997**, 74, 258–263.
28. Pomes, A. F. Zein, in *Encyclopedia of Polymer Science and Technology: Plastics, Resins, Rubbers, Fibers*, ed. H. F. Mark, N. G. Gaylord and N. M. Bikales, Interscience Publishers, New York, **1971**, vol. 15, pp. 125–132.
29. Kovacs, I.; Lundany, A.; Köszegi, T.; Feher, J.; Kovacs, B.; Szolcsanyi, J.; Pinter, E. *Neuropeptides*. **2005**, 39, 395–402.
30. Schenkels, L. C. P. M.; Veerman, E. C. I.; Amerongen, A. V. N. *Crit. Rev. Oral Biol. Med.* **1995**, 6, 161–175.
31. Yasui, T.; Fukui, K.; Nara, T.; Habata, I.; Meyer, W.; Tsukise, A. *Arch. Dermatol. Res.* **2007**, 299, 393–397.
32. Lu, J. R.; Su, T. J.; Howlin, B. J. *J. Phys. Chem. B*. **1999**, 103, 5903–5909.
33. Harbury, H. A.; Loach, P. A. *J. Biol. Chem.* **1960**, 235, 3640–3645.
34. Ganzevles, R. A.; Zinoviadou, K.; van Vliet, T.; Cohen Stuart, M. A.; de Jongh, H. H. *J. Langmuir*. **2006**, 22, 10089–10096.
35. Knott, B. C.; Crowley, M. F.; Himmel, M. E.; Ståhlberg, J.; Beckham, G. T. *J. Am. Chem. Soc.* **2014**, 136, 8810–8819.
36. Li, J.; Yu, S.; Yao, P.; Jiang, M. *Langmuir*. **2008**, 24, 3486–3492.
37. Antonov, Y. A.; Wolf, B. A. *Biomacromolecules*. **2005**, 6, 2980–2989.
38. Thomas, J. J.; Rekha, M. R.; Sharma, C. P. *Mol. Pharmaceutics*, **2011**, 9, 121–134.
39. Yoo, S. H.; Lee, K. H.; Lee, J. S.; Cha, J.; Park, C. S.; Lee, H. G. *J. Agric. Food Chem.* **2005**, 53, 6235–6239.
40. Dorsey, J. G.; Cooper, W. T.; Siles, B. A.; Foley, J. P.; Barth, H. G. *Anal. Chem.* **1998**, 70, 591R–644R.
41. Larive, C. K.; Lunte, S. M.; Zhong, M.; Perkins, M. D.; Wilson, G. S.; Gokulrangan, G.; Williams, T.; Afroz, F.; Schoneich, C.; Derrick, T. S.; Middaugh, C. R.; Bogdanowich-Knipp, S. *Anal. Chem.* **1999**, 71, 389–423.
42. Westbrook, S. I.; McDowell, G. H. *Aust. J. Agric. Res.* **1994**, 45, 1693–1700.
43. Joo, I.; Emod, J. *Vaccine*, **1988**, 6, 233–237.
44. Fox, R. M.; Mynderse, J. F.; Goulian, M. *Biochemistry*. **1977**, 16, 4470–4477.
45. Rigby, P. *Nature*. **1969**, 221, 968.
46. Liptay, S.; Weidenbach, H.; Adler, G.; Schmid, R. M. *Digestion*. **1998**, 59, 142–147.
47. Gavalas, V. G.; Chaniotakis, N. A. *Anal. Chim. Acta*. **2000**, 404, 67–73.
48. Ghimici, L.; Constantin, M.; Fundueanu, G. *Mater.* **2010**, 181, 351–358.
49. Ghimici, L.; Morariu, S.; Nichifor, M. *Sep. Purif. Technol.* **2009**, 68, 165–171.
50. Goshisht, M. K.; Moudgil, L.; Rani, M.; Khullar, P.; Singh, G.; Kumar, H.; Singh, N.; Kaur, G.; Bakshi, M. S. *J. Phys. Chem. C*. **2014**, 118, 28207–28219.
51. Mahal, A.; Goshisht, M. K.; Khullar, P.; Kumar, H.; Singh, N.; Kaur, G.; Bakshi, M. S. *Phys. Chem. Chem. Phys.* **2014**, 16, 14257–14270.
52. Mahal, A.; Khullar, P.; Kumar, H.; Kaur, G.; Singh, N.; Jelokhani-Niaraki, M.; Bakshi, M. S. *ACS Sustainable Chem. Eng.*, **2013**, 1, 627–639.
53. Hattori, A.; Umetsu, M.; Nakanishi, T.; Sawai, S.; Kikuchi, S.; Asano, R.; and Kumagai, I. *Bioconjugate Chem.* **2012**, 23, 1934–1944.
54. Manikas, A. C.; Causa, F.; Moglie, R. D.; and Netti, P. A. *ACS Appl. Mater. Interfaces*. **2013**, 5, 7915–7922.
55. Burt, J. L.; Gutierrez-Wing, C.; Miki-Yoshida, M.; and Jos-Yacamán, M. *Langmuir*, **2004**, 20, 11778–11783.
56. Bakshi, M. S.; Kaur, H.; Khullar, P.; Banipal, T. S.; Kaur, G.; and Singh, N. *J. Phys. Chem. C*. **2011**, 115, 2982–2992.
57. Bakshi, M. S. *J. Phys. Chem. C*, **2011**, 115, 13947–13960.
58. Mahal, A.; Khullar, P.; Kumar, H.; Kaur, G.; Singh, N.; Jelokhani-Niaraki, M.; and Bakshi, M. S. *ACS Sustainable Chem. Eng.* **2013**, 1, 627–639.
59. Berendsen, H. J. C.; Van der Spoel, D.; Van Drunen, R. *Comput. Phys. Commun.* **1995**, 91, 43–56.
60. Iori, F.; Felice, R. D.; Molinari, E.; Corni, S. *J. Comput. Chem.* **2009**, 30, 1465–1476.
61. Hoefling, M.; Iori, F.; Corni, S.; Gottschalk, K. E. *Langmuir*, **2010**, 26, 8347–8351.
62. Bernstein, F. C.; Koetzle, T. F.; Williams, G. J. B.; Meyer, E. F.; Brice, M. D.; Roger, J. R. *J. Mol. Biol.* **1977**, 112, 535–542.
63. Berendsen, H. J. C.; Postma, J. P. M.; Van Gunsteren, W. F.; Hermans, J. *Interaction Models for Water in Relation to Protein Hydration*. In *Intermolecular Forces*; Pullman, B., Ed.; D Reidel Publishing Company: Dordrecht, The Netherlands, **1981**; pp 331–342.
64. Hess, B.; Bekker, H.; Berendsen, H. J. C.; Fraaije, J. G. E. M. *J. Comput. Chem.* **1997**, 18, 1463–1472.
65. Darden, T.; York, D.; Pedersen, L. *J. Chem. Phys.* **1993**, 98, 10089–10092.
66. Bakshi, M. S. *Langmuir*. **2009**, 25, 12697–12705.
67. Bakshi, M. S. *J. Phys. Chem. C*. **2011**, 115, 13947–13960.
68. Khullar, P.; Singh, V.; Mahal, A.; Dave, P. N.; Thakur, S.; Kaur, G.; Singh, J.; Kamboj, S.; Bakshi, M. S. *J. Phys. Chem. C*. **2012**, 116, 8834–8843.
69. Baker, N. A.; Sept, D.; Joseph, S.; Holst, M. J.; McCammon, J. A. *Proc. Natl. Acad. Sci. U. S. A.* **2001**, 98, 10037–10041.
70. Gray, J. J. *Curr. Opin. Struct. Biol.* **2004**, 14, 110–115.

71. Rabias, I.; Tsitrouli, D.; Karakosta, E.; Kehagias, T.; Diamantopoulos, G.; Fardis, M.; Stamopoulos, D.; Maris, T. G.; Falaras, P.; Zouridakis, N. *Biomicrofluidics*. **2010**, *4*, 024111–024119.
72. Peelle, B. R.; Krauland, E. M.; Wittrup, K. D.; Belcher, A. M. *Langmuir*, **2005**, *21*, 6929–6933
73. Hnilova, M.; oren, E. E.; Seker, U. O. S.; Wilson, B. R.; Collino, S.; Evans, J. S.; Tamerler, C.; Sarikaya, M. *Langmuir*, **2008**, *24*, 12440–12445.
74. Sato, T.; Kamachi, M.; Mizusaki, M.; Yoda, K.; Morishima, Y. *Macromolecules*. **1998**, *31*, 6871–6877.
75. Sato, T.; Mattison, K. W.; Dubin, P. L.; Kamachi, M.; Morishima, Y. *Langmuir*. **1998**, *14*, 5430– 5437.
76. Tran, J. C.; Doucette, A. A. *J. Proteome Res.* **2008**, *7*, 1761–1766.
77. Lin, Y. S.; Haynes, C. L. *J. Am. Chem. Soc.* **2010**, *132*, 4834–4842.
78. Lin, Y. S.; Haynes, C. L. *Chem. Mater.* **2009**, *21*, 3979–3986.
79. Neumann, D. Z.; Wang, H.; Yuwono, V. M.; Barhoumi, A.; Perham, M.; Hartgerink, J. D., Wittung- Stafshede, P.; and Halas, N. J. *Nano Lett.* **2009**, *9*, 666.
80. de Groot, N. S.; and Ventura, S. *Spectroscopy*. **2005**, *19*, 199.
81. Pertinhez, T. A., Bouchard, M.; Tomlinson, E. T.; Wain, R.; Ferguson, S. J.; Dobson, C. M.; and Smith, L. J. *FEBS Lett.* **2001**, *495*, 184.
82. Zhao, Y.; Sun, X.; Zhang, G.; Trewyn, B. G.; Slowing, I. I.; and Lin, V. S. Y. *ACS Nano*. **2011**, *5*, 1366–1375.
83. Yu, T.; Malugin, A.; and Ghandehari, H. *ACS Nano*, **2011**, *5*, 5717–5728.
84. Bugarin, D.; Grbovic, S.; Orcic, D.; Mitic- Culafic, D.; Knezevik Vukcevic, J.; Mimica- Dukic, N. *Molecules*, 2014, *19* (11), 19007–20.
85. Liao, R. S.; Rennie, R. P.; and Talbot, J. A. *J. ClinMicrobiol.* **2001**, *39*(7), 2708–2712.